Korean J. Chem. Eng., 33(4), 1416-1424 (2016)
DOI: 10.1007/s11814-015-0248-y

pISSN: 0256-1115
eISSN: 1975-7220

Removal of Cr(VI) from aqueous solution by rice husk derived magnetic sorbents

Yuan Fan, Ruifeng Yang†, Zhimin Lei, Na Liu, Jialiang Lv, Shangru Zhai†, Bin Zhai, and Lei Wang

Faculty of Light Industry and Chemical Engineering, Dalian Polytechnic University, Dalian 116034, China
(*Received 26 August 2015 • accepted 17 November 2015*)

Abstract−A novel magnetic porous sorbent obtained from agricultural waste rice husk was successfully synthesized through a simple carbon-thermal method. The sorbent was characterized by scanning electron microscopy, transmission electron microscopy, X-ray diffraction, Fourier transform infrared spectroscopy, vibrating sample magnetometer, N_2 sorption analysis, and X-ray photoelectron spectroscopy. The removal efficiency of the sorbent for Cr(VI) was also investigated. Chromium adsorption was fitted by the pseudo-second-order and Langmuir models. The maximum chromium adsorption capacity, Brunauer-Emmett-Teller surface area, and average Barrett-Joyner-Halenda pore size of the magnetic sorbent were 157.7 $mg \cdot g^{-1}$, 134.1 $m^2 \cdot g^{-1}$, and 4.99 nm, respectively. The saturated magnetization of the novel adsorbent was 77.8 $emu \cdot g^{-1}$, indicating that the material can facilitate separation and recovery from aqueous systems. The removal mechanisms of Cr(VI) were also discussed. The result illustrates that rice husk-derived magnetic carbonaceous materials are a potential adsorbent for Cr(VI) pollution treatment and provide a suitable method for the effective conversion of biomass waste, which may solve the problem of waste disposal and widen the applications of the materials.

Keywords: Bio-sorbent, Magnetic, Cr(VI) Removal, Adsorption, Agricultural Waste

INTRODUCTION

Reliable access to clean natural water sources or drinking water is an important global issue. Continuous industrialization and urbanization have triggered a number of environmental problems. Given their complexity and persistence, toxic organic dyes and heavy metal pollution pose a serious threat to human health and the environment [1-9]. The toxic metal Cr is generated by the electroplating, leather tanning, printing, cement, and mining industries, among others [10,11]. The presence of Cr(VI) species in drinking water not only exerts detrimental effects on the aquatic ecosystem but also increases the risk of severe diarrhea and bladder, liver, kidney, and skin cancers [12]. Hence, the removal of Cr(VI) from aqueous solutions is a chief concern.

Numerous water purification and treatment methods have been developed [13]. Adsorption is one of the most economically practical and technically simple methods [14]. Adsorbents obtained from agricultural wastes or by-products have attracted considerable research attention because of their low cost, availability, abundance, and renewability. Consequently, many low-cost adsorbents for wastewater treatment have been studied [15-27]. Rice husk (RH) is an abundant agriculture residue in rice-producing countries, with its global annual production reaching roughly 80 million tons, of which half is produced in China [28]. Thus, the efficient utilization of RH rather than wasting and burning poses a challenge. Fortunately, the unique properties, ecological safeness, and low cost of RH have rendered this material a promising adsorbent for Cr(VI) removal. Low et al. [29] demonstrated that quaternized rice hulls remove Cr(VI) better than untreated rice hulls over the pH range of pH 2-10. Guo et al. [30] prepared RH-based activated carbon with a high specific surface area through KOH and NaOH activation at low temperatures and found that the resulting adsorbent exhibits a large adsorption capacity toward Cr(VI). Bishnoi et al. [31] utilized activated RH carbon as an adsorbent for Cr(VI) treatment. Li et al. [32] used RH as a carbon source to synthesize nitrogen-doped porous carbon combined with magnetic nanocomposites for Cr(VI) adsorption and found that the material displays excellent adsorption. However, to the best of our knowledge, Cr(VI) removal using RH-based magnetic carbonaceous adsorbents has received minimal attention. Numerous magnetic carbon-based adsorbents, such as magnetic graphene, magnetized activated carbon, and magnetic carbon nanotubes, have been fabricated, but highly efficient waste RH-derived Cr(VI) adsorbents that possess a large adsorption capacity and allow simple separation have yet to be developed.

In contrast to traditional adsorbents, magnetic carbonaceous adsorbents can conveniently be separated from treated water via a simple magnetic process [33].Various methods, such as hydrothermal carbonization method [34], pyrolysis [35], and microwave-assisted pyrolysis [36], have been used to fabricate magnetic carbons. Among these, pyrolysis has been extensively studied because of its simple operation [37]. Qiu et al.[38] have recently synthesized a magnetic carbon with a zero-valence iron(ZVI)/Fe_3O_4 core through calcination, with cellulose and $Fe(NO_3)_3$ as carbon and iron precursors, respectively. They observed that the synthesized magnetic carbon performs Cr(VI) removal superbly. RH is mainly composed of cellulose, hemicellulose, lignin, and silica. However, the presence of silica and other surface impurities affects the chemical and physical adsorption properties of RH [39]. Alkali (NaOH) treatment of RH improves the adsorption properties of the material [40] by removing natural fats, amorphous silica, waxes, and

†To whom correspondence should be addressed.
E-mail: yangrf@dlpu.edu.cn, zhaisr@dlpu.edu.cn

low-molecular-weight lignin compounds from the RH and consequently revealing several available hydroxyl groups and other reactive functional groups. These findings indicate that cellulose-containing RH can be used as a carbon precursor to fabricate magnetic carbon.

Significant efforts have been exerted toward RH disposal and resource recovery. For instance, silica microspheres were prepared using NaOH-extracted silicates and lignin species from RHs [41], and solid RH residue was transformed into high-performance activated carbons for the removal of dye from wastewater [42]. Porous carbons have also been prepared from NaOH-pretreated RHs by coupling low-temperature solution-processed carbonization and H_3PO_4 activation [43]. However, cellulose-containing RH has never been used as a carbon precursor to fabricate magnetic adsorbents, and the potential of these adsorbents for Cr(VI) removal has not been explored. In the present study, solid RH residue (i.e., NaOH-treated RH) and $FeCl_3{\cdot}6H_2O$ were used as carbon and iron precursors, respectively, to prepare new magnetic adsorbents via a simple carbon-thermal method. In addition, porous carbon with magnetic nanoparticles formed in situ was fabricated. Transforming waste RHs into magnetic adsorbents is an incremental advance at best. The prepared magnetic carbonaceous materials have the advantages of simple preparation, desirable magnetic properties, large adsorption capacity, and low cost, making them promising adsorbents for Cr(VI) removal. The synthetic adsorbent was characterized via scanning electron microscopy (SEM), transmission electron microscopy (TEM), X-ray diffraction (XRD), Fourier transform infrared (FTIR) spectroscopy, vibrating sample magnetometer (VSM), N_2 sorption, and X-ray photoelectron spectroscopy (XPS). The removal efficiency of the adsorbent for Cr(VI) was also investigated. The effects of solution pH, contact time, different weight ratios ($m_{solid\ RH\ residue}/m_{FeCl_3\cdot 6H_2O}$), and temperature were evaluated in detail.

EXPERIMENTAL

1. Materials

RH was obtained from a rice mill near Dalian, Liaoning Province, China. The material was washed using distilled water to remove adhering soil, dried in an oven at 100 °C overnight, milled into powder, and then sieved through a 60-mesh sieve. $FeCl_3{\cdot}6H_2O$, HCl, NaOH, H_3PO_4, and ethanol were purchased from Tianjin Kermel Co., Ltd., China. $K_2Cr_2O_7$ and 1,5-diphenylcarbazidewerepurchased from Sinopharm Chemical Reagent Co., Ltd., China. All chemical reagents used were analytical grade. Deionized water was used throughout the experiment.

2. Preparation of a Carbonaceous Precursor

Cleaned RH powder and 2 M NaOH were mixed at a ratio of 1 : 7 (w/v) in a 500 mL three-neck round-bottom flask equipped with a thermometer and then heated to 100 °C for 4 h. Solid RH residue was collected by vacuum filtration, repeatedly washed with deionized water until the wash water become neutral and then dried at 120 °C overnight.

3. Preparation of a Magnetic Carbonaceous Adsorbent

A magnetic carbon-based adsorbent was synthesized using a simple carbon-thermal method. In brief, 10.0 g of $FeCl_3{\cdot}6H_2O$ was dissolved in 50 mL of ethanol with stirring at room temperature for 30 min. Afterward, 5.0 g of solid RH residue was added with the $FeCl_3{\cdot}6H_2O$ solution, and the mixture was vigorously stirred for 2 h to distribute Fe^{3+} homogeneously within the carbonaceous materials. The mixture was placed in a water bath at 50 °C to evaporate ethanol completely, and the remaining solid was dried at 100 °C for 24 h in a drying oven. The resulting products were placed in a tube furnace, heated to 800 °C at a rate of 5 °C·min^{-1} under N_2 atmosphere, and then stored for 2 h. After cooling to room temperature, the RH-derived magnetic adsorbent was ground into powder, collected by a magnet, washed with deionized water until clear, and then dried in a vacuum oven at 80 °C. The obtained sample was denoted as RHC-Mag-2.

Different weight ratios of $FeCl_3{\cdot}6H_2O$/solid RH residue ($FeCl_3{\cdot}6H_2O$: solid RH residue=0.5 : 1, 1 : 1) were fabricated by using the process described above to investigate the role of Fe(III) salt in the preparation of the magnetic adsorbent. The acquired products were denoted as RHC-Mag-0.5 and RHC-Mag-1.

4. Characterization

The morphology and microstructure of the magnetic adsorbent were analyzed by SEM (JSM-6460LV electron microscope, JEOL, Japan) and TEM (JEM-2000EX electron microscope, JEOL, Japan). XRD patterns were recorded on a Shimadzu XRD-6100 diffractometer with CuKα radiation (λ=1.54060 Å) from 10° to 80° at a scanning speed of 8°·min^{-1}. The functional groups were evaluated using FTIR spectroscopy (Perkin-Elmer, USA) in the 4,000-400 cm^{-1} region. Magnetism was measured with a Lake Shore 7410 VSM at room temperature. The textural properties, including specific surface area, total pore volume, and pore size, of the samples were evaluated by performing nitrogen adsorption-desorption experiments at 77 K (Quantachrome Autosorb NOVA2200e, USA). XPS was conducted using a Thermo Scientific ESCALAB250 spectrometer (Thermo VG, USA) equipped with an Al-Ka X-ray source (1486.6 eV).

5. Cr(VI) Adsorption Experiments

A stock solution containing 1,000 mg·L^{-1} Cr(VI) was prepared by dissolving 2.829 g of $K_2Cr_2O_7$ in 1,000 mL of deionized water. Solutions with the required concentrations were obtained by diluting the stock solution. Batch experiments were performed on 50 mL conical flasks, each containing 20 mL of Cr(VI) aqueous solution. The adsorbent (0.02 g) was added to each flask and then shaken for a specified period. The effect of pH was investigated over a pH range of 2.0-11.0 with an initial Cr(VI) concentration of 50 mg·L^{-1} at room temperature. The pH value was adjusted using a 1 M HCl or 1 M NaOH solution with a pH meter (pHS-3C, Shanghai, China). Kinetic experiments were conducted at pH 2.0 with 50 and 100 mg·L^{-1} Cr(VI) solutions at designated time periods. For the adsorption isotherm tests, the adsorption of Cr(VI) was carried out with initial concentrations ranging from 50 mg·L^{-1} to 300 mg·L^{-1} for 24 h at pH 2.0. The experiments were at different temperatures of 298, 308, and 318 K. After adsorption, the mixture was filtered through a 0.22 μm membrane filter. The concentrations of Cr(VI) were analyzed using an ultraviolet-visible light spectrophotometer (Agilent Cary 60 spectrophotometer) at a wavelength of 540 nm with a colorimetric method using 1,5-diphenylcarbazide. The equilibrium adsorption capacity q_e (mg·g^{-1}) and the removal efficiency (%R) were calculated as follows:

$$q_e = \frac{(C_0 - C_e)V}{m} \quad (1)$$

$$\%R = \frac{(C_0 - C_e)}{C_0} \times 100\%, \quad (2)$$

where C_0 and C_e ($mg \cdot L^{-1}$) are the initial and equilibrium Cr(VI) concentrations in the aqueous solution, respectively, V (L) is the volume of the solution, and m (g) is the mass of the adsorbent. The error bars represent the standard deviation estimated from three determinations.

RESULTS AND DISCUSSION

1. Characterization

The SEM images of pristine RH and RHC-Mag-2 are shown in Figs. S1(a) and (b), respectively. Pristine RH exhibited a rough surface and inconspicuous pore structure. By contrast, spherical particles with an uneven distribution were observed in RHC-Mag-2, indicating the successful introduction of Fe_3O_4 particles on the surface of the carbonaceous material despite their slight aggregation. Detailed structural information of RHC-Mag-2 was further obtained using TEM (Fig. S1(c)). RHC-Mag-2 was irregularly shaped, with Fe_3O_4 particles deposited on the carbonaceous precursor. This finding suggested that the inorganic salt $FeCl_3 \cdot 6H_2O$ was successfully transformed to nanoparticles, resulting in a magnetic carbonaceous material as expected.

The composition and crystal nature of RHC-Mag-2 were investigated using XRD. As shown in Fig. S2, the diffraction peak at 26.2° corresponded to the (002) plane of the graphite structure, which was due to the formation of carbon structures with some degree of graphitic order during carbonization under high temperature [44]. The diffraction peaks at 30.1°, 35.5°, 43.3°, 53.7°, 57.2°, and 62.8° belong to the (220), (311), (400), (422), (511), and (440) reflections of Fe_3O_4, respectively [45]. Moreover, the diffraction at 44.7° was assigned to the (100) plane of cubic Fe [38]. These results demonstrated that Fe_3O_4 nanoparticles were introduced during calcinations and that Fe^{3+} was partly reduced to ZVI, which is important for Cr(VI) removal. Thus, solid RH residue is a good carbon precursor for the synthesis of magnetic carbon-based adsorbents.

The functional groups of RH, RHC-Mag-2, and after Cr(VI) adsorption on RHC-Mag-2 were characterized by FTIR spectroscopy. The typical spectra of pure RH are shown in Fig. S3(a). The strong adsorption peak at 3,435 cm^{-1} was due to the stretching vibration of -OH. The peaks located at 2,924 and 2,850 cm^{-1} corresponded to the C-H stretching vibration. The peaks at 1,631 and 1,384 cm^{-1} were attributed to aromatic ring vibration and $-CH_3$ groups, respectively. The band at 1,095 cm^{-1} was characteristic of the Si-O-Si bond, whereas the band at 801 cm^{-1} was associated with the Si-O bond. RHC-Mag-2 exhibited an FTIR spectrum similar to that of RH (Fig. S3(b)). However, changes were observed in RHC-Mag-2. Notably, the peak at 3,426 cm^{-1}, which was assigned to -OH, was broad. Moreover, the discernible peak at 590 cm^{-1} was related to Fe-O stretching vibration. These results revealed that Fe_3O_4 particles were successfully installed on the carbonaceous precursor, which was consistent with the SEM and XRD analyses. Fig. S3(c) illustrates the spectra of RHC-Mag-2 after Cr(VI) adsorption. Changes after interaction with Cr(VI) were less visible. The peak at 3,426 cm^{-1} shifted to 3,424 cm^{-1} after Cr(VI) adsorption, which implies that the -OH groups might play an important role in Cr(VI) adsorption.

Magnetic measurement of RHC-Mag-2 was performed using a vibrating sample magnetometer at room temperature. As demonstrated in Fig. 1(a), the as-prepared RHC-Mag-2 exhibited good magnetic properties with a saturation magnetization of 77.8 $emu \cdot g^{-1}$. Thus, this material is capable of magnetic separation and recovery. The insets in Fig. 1(a) show that the synthesized RHC-Mag-2 can be collected in less than 30 s by using a permanent magnet from the treated solution, confirming their magnetic nature.

The textural characteristics of RH and RHC-Mag-2 calculated from nitrogen adsorption-desorption isotherms are depicted in Fig. 1(b). RHC-Mag-2 was of representative type-IV curves with hysteresis loops, which is typical for mesoporous materials. As shown in Table S1, the Brunauer–Emmett–Teller surface area of RHC-Mag-2 (134.1 $m^2 \cdot g^{-1}$) was significantly higher than that of RH (9.1 $m^2 \cdot g^{-1}$). The average pore diameters of RH and RHC-Mag-2 were

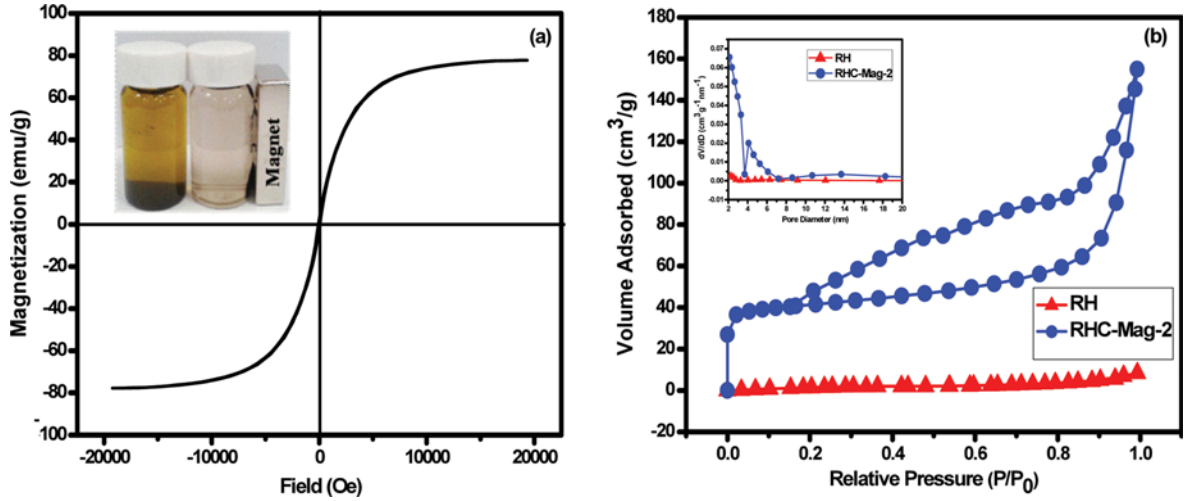

Fig. 1. Magnetization curve of RHC-Mag-2 (a); N_2 adsorption-desorption isotherms and pore size distribution curves of RH, RHC-Mag-2 (b).

approximately 8.26 and 4.99 nm, respectively. These properties indicated that RHC-Mag-2 was potentially beneficial for Cr(VI) removal from aqueous systems.

2. Adsorption of Cr(VI) over Prepared Sorbents

2-1. Effect of pH

Solution pH plays a crucial role in Cr(VI) removal by influencing the existing form of chromium and the property of adsorbents. Fig. S4 presents the results of Cr(VI) removal percentages by RHC-Mag-2 with the initial solution pH within 2.0-11.0 at an initial Cr(VI) concentration of 50 mg·L^{-1}. The removal percentage of Cr(VI) by RHC-Mag-2 rapidly decreased with increasing pH; this result agrees with previous findings.RHC-Mag-2 facilitated ~100% removal of Cr(VI) at pH 2.0, but this rate was only ~20% at pH 11.0. The solution pH markedly influenced Cr(VI) removal. Cr(VI) in aqueous solutions exists in various forms, such as$HCrO_4^-$, $Cr_2O_7^{2-}$, and CrO_4^{2-}, which are related to solution pH and total Cr(VI) concentration [46]. The predominant species at pH 2.0-5.0 is $HCrO_4^-$, whereas that at high pH values is CrO_4^{2-}. $HCrO_4^-$ preferentially adsorbs on the carbon surface because of its low adsorption free energy [47]. A large amount of H^+ is present at low pH, contributing to the positive charge of the RHC-Mag-2 surface. Thus, anionic species of Cr(VI) can easily be adsorbed onto the RHC-Mag-2 surface through electrostatic attraction. However, the increasing concentration of OH^- ions with increasing pH introduced competitive adsorption with Cr(VI) species. As a result, RHC-Mag-2 exhibited a much lower removal efficiency at higher-pH solutions.

2-2. Adsorption Kinetics

The time profiles of Cr(VI) removal with RHC-Mag-2 at two initial Cr(VI) concentrations (50 and 100 mg·L^{-1}) are illustrated in Fig. 2. The adsorption capacity of RHC-Mag-2 on Cr(VI) steeply increased at the initial stage because of the presence of more available binding sites for Cr(VI). Thereafter, the rate of increase in adsorption slowed down before finally reaching the equilibrium. The time needed to reach the equilibrium was correlated with the relevant initial concentrations. At 50 mg·L^{-1}, the adsorption of Cr(VI) reached the equilibrium in approximately 90 min. The equilibrium adsorption capacities of RHC-Mag-2 in 50 and 100 mg·L^{-1} Cr(VI) solutions were 49.913 and 99.158 mg·g^{-1}, respectively. The amount of Cr(VI) adsorbed by RHC-Mag-2 enhanced with increasing initial Cr(VI) concentration because of the higher initial concentration resulting from faster and stronger binding sites. Furthermore,

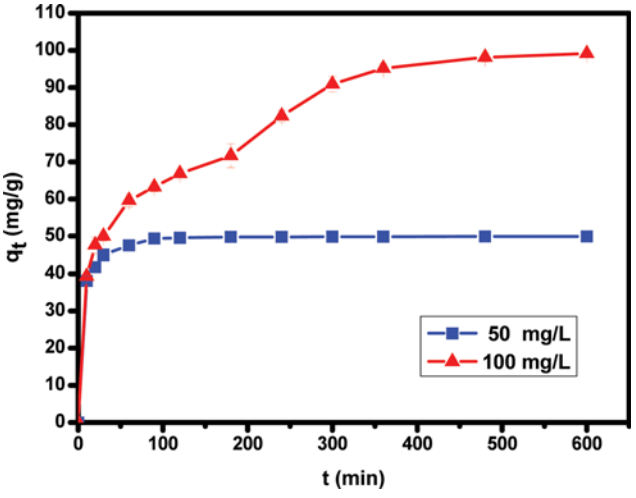

Fig. 2. Effect of the contact time on Cr(VI) adsorption at different initial concentrations of 50 and 100 mg/L (adsorbent dose, 0.02 g; volume, 20 mL; pH, 2.0 and temperature, 298 K).

Table 1. Kinetic parameters for adsorption of Cr(VI) onto RHC-Mag-2

Initial concentrations (mg L^{-1})	Kinetic parameters	
	50	100
$q_{e,exp}$ (mg g^{-1})	49.913	99.158
Pseudo-first-order model		
$q_{e,cal}$ (mg g^{-1})	15.107	60.763
k_1 (min^{-1})	0.0323	0.006
R^2	0.9523	0.9403
Pseudo-second-order model		
$q_{e,cal}$ (mg g^{-1})	50.150	98.619
k_2 (g mg^{-1} min^{-1})	0.0100	0.0005
R^2	0.9999	0.9856

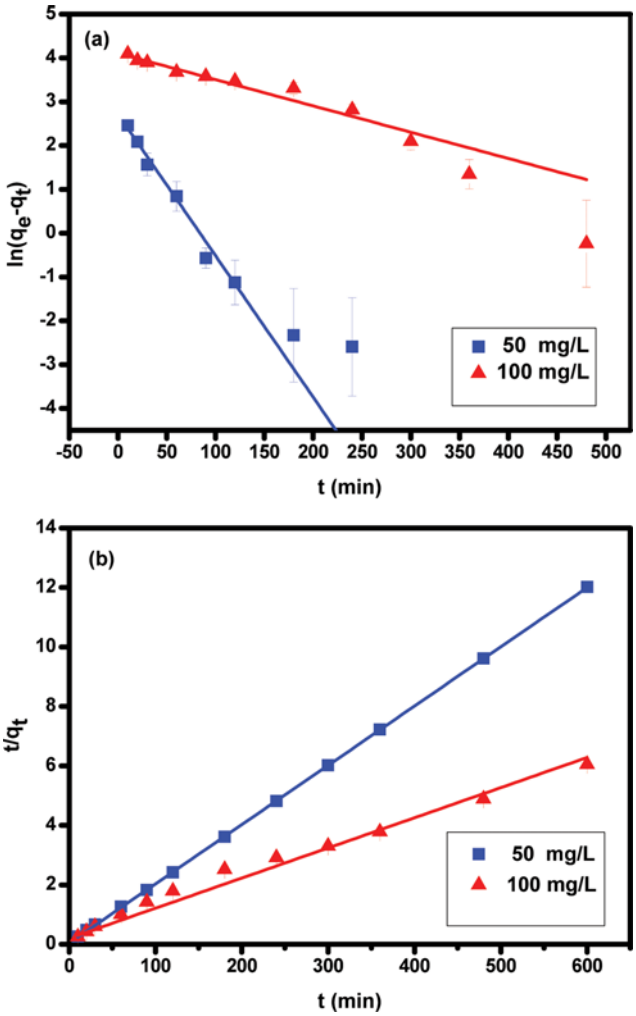

Fig. 3. Pseudo-first-order kinetic model (a), pseudo-second-order kinetic model (b) for adsorption of Cr(VI) onto RHC-Mag-2.

the pseudo-first-order and pseudo-second-order models were tested to study the kinetics of Cr(VI) adsorption. The models can be expressed as follows [48]:

$$\ln(q_e - q_t) = \ln q_e - k_1 t \quad (3)$$

$$\frac{t}{q_t} = \frac{1}{k_2 q_e^2} + \frac{t}{q_e}, \quad (4)$$

where q_e and q_t are the adsorption capacity of metal ions at equilibrium and at time t, respectively, and k_1 (min^{-1}) and k_2 ($g \cdot mg^{-1} \cdot min^{-1}$) are the rate constants of the pseudo-first-order and pseudo-second-order models, respectively.

Table 1 lists the corresponding kinetic parameters for the two models obtained by linear regression (Figs. 3(a) and (b)). The pseudo-second-order model provided higher correlation coefficients compared with the pseudo-first-order model. Moreover, the calculated q_e values ($q_{e,cal}$) of the pseudo-second-order model agreed with the experimental values. This result indicates that Cr(VI) adsorption on RHC-Mag-2 fits the pseudo-second-order model.

2-3. Effect of the Fe(III) Salt: Solid RH Residue Ratio

The Fe(III) salt to solid RH residue ratio is a key factor affecting magnetic adsorbent synthesis. The effect of the Fe(III) salt : solid RH residue ratio on Cr(VI) adsorption was studied by varying this ratio from 0.5 : 1 to 2 : 1 in magnetic adsorbent synthesis, and the results are shown in Fig. 4. The adsorption capacities of Cr(VI) increased with increasing Fe(III) salt content. This result revealed that Fe(III) salt content played a crucial role in Cr(VI) adsorption. This finding may be attributed to the fact that Fe(III) can be transformed into a magnetic material through the carbon-thermal method, in which ZVI and Fe_3O_4 as electron donors can remove Cr(VI) from water [49]. Meanwhile, Fe(III) showed a strong affinity for Cr(VI) through chemical adsorption [50]. Hence, higher proportions of Fe(III) exhibited higher adsorption abilities. In addition, $FeCl_3$ as an activation agent can catalyze the formation of a porous structure under carbonization conditions, thereby producing a high surface area [51]. The higher proportion of Fe(III) might have resulted in a higher surface area, which offered more binding sites, leading to higher amounts of Cr(VI) removed. Two common isotherm models, the Langmuir and Freundlich models, were applied to fit the experimental data as follows [52,53]:

$$\frac{C_e}{q_e} = \frac{C_e}{q_{max}} + \frac{1}{q_{max} \cdot b} \quad (5)$$

$$\log q_e = \log K_f + \frac{1}{n} \log C_e, \quad (6)$$

where C_e is the equilibrium concentration ($mg \cdot L^{-1}$), q_e is the equilibrium adsorption capacity ($mg \cdot g^{-1}$), q_{max} is the maximum adsorption capacity ($mg \cdot g^{-1}$), b is the equilibrium constant ($L \cdot mg^{-1}$), and K_f and n are adsorption constants related to adsorption capacity and adsorption intensity, respectively.

The linear plots of the two isotherm models are shown in Figs. 5(a) and (b), and the results are presented in Table S2. Based on the correlation coefficients (R^2), the Cr(VI) adsorption isotherms by RHC-Mag-0.5, RHC-Mag-1, and RHC-Mag-2 fit better with the Langmuir model than with the Freundlich model, suggesting a monolayer adsorption process. The maximum adsorption capacities

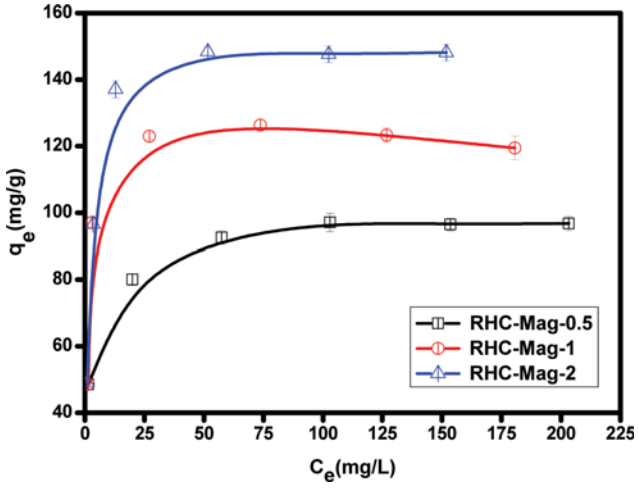

Fig. 4. Adsorption isotherms of Cr(VI) on RHC-Mag-0.5, RHC-Mag-1 and RHC-Mag-2 (adsorbent dose, 0.02 g; volume, 20 mL; pH, 2.0 and contact time 24 h).

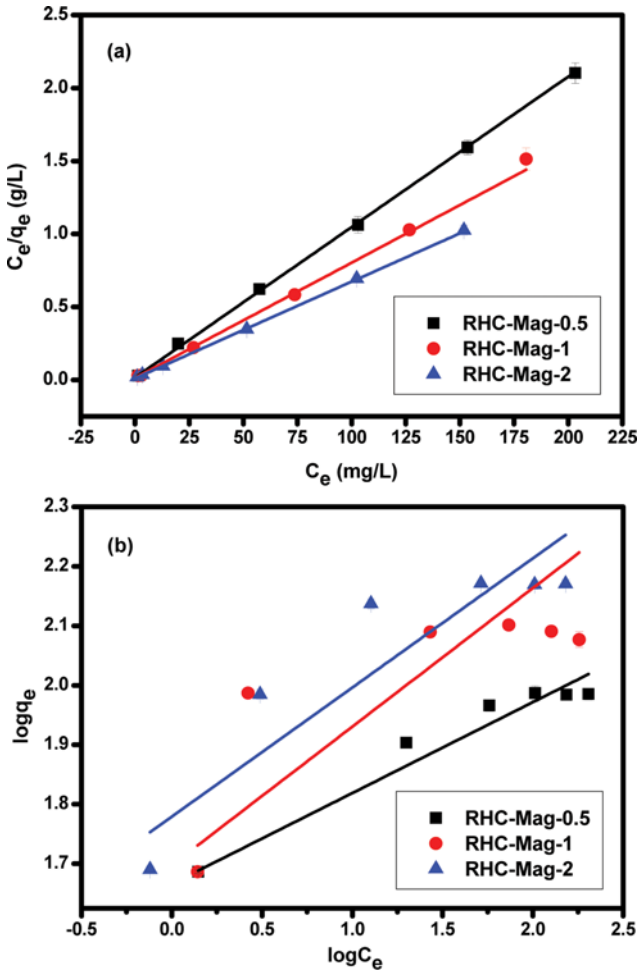

Fig. 5. Linear plots of (a) Langmuir model and (b) Freundlich model of the Cr(VI) adsorption onto RHC-Mag-0.5, RHC-Mag-1 and RHC-Mag-2.

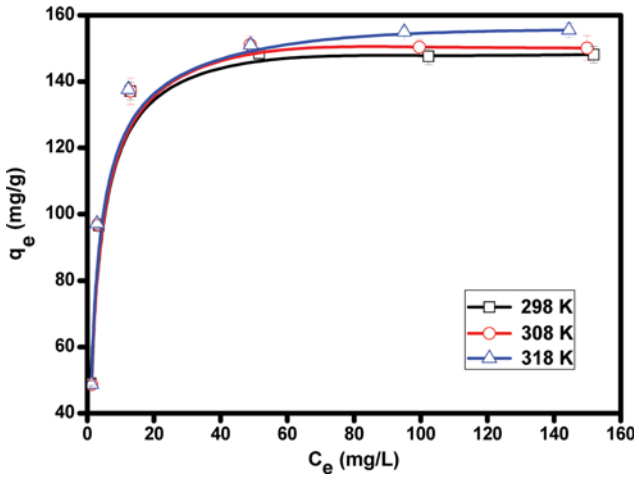

Fig. 6. Adsorption isotherms of Cr(VI) on RHC-Mag-2 at different temperatures of 298 K, 308 K, and 318 K (adsorbent dose, 0.02 g; volume, 20 mL; pH, 2.0 and contact time 24 h).

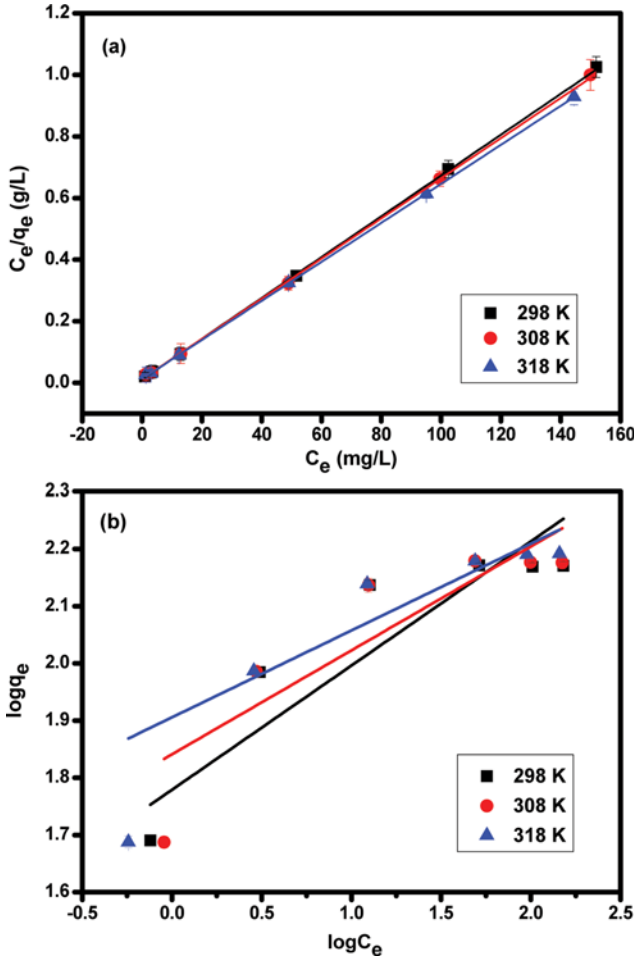

Fig. 7. (a) Langmuir and (b) Freundlich isotherm plots for adsorption of Cr(VI) onto RHC-Mag-2 at different temperatures.

of Cr(VI) on RHC-Mag-0.5, RHC-Mag-1, and RHC-Mag-2 calculated from the Langmuir model were 96.993, 126.582, and 150.830 mg·g^{-1}, respectively, which indicated high adsorption abilities.

Table 2. Comparison of Cr(VI) adsorption capacities with other adsorbents

Adsorbent	q_{max} (mg g^{-1})	References
Quaternized rice hulls	32.3	[29]
N-doped Fe_3O_4/carbon	16.0	[32]
Magnetic carbon	327.5	[38]
Fe_3O_4/CNT-IL	55.43	[55]
Magnetized activated carbon	57.37	[56]
RHC-Mag-2	157.729	This study

2-4. Effect of Temperature

The effect of temperature on Cr(VI) removal was also investigated. The adsorption capacity of RHC-Mag-2 for Cr(VI) was slightly influenced by temperature (Fig. 6). The amount of adsorbed Cr(VI) increased with increasing temperature from 298 K to 318 K.

Moreover, the Cr(VI) adsorption data were fitted using the Langmuir and Freundlich isotherms (Fig. 7). The relevant parameters obtained from the isotherms are summarized in Table 2. The isotherm data at three temperatures were better fit by the Langmuir model than the Freundlich model, as indicated by the relatively higher correlation coefficient (R^2) of the former than the latter. This finding indicated the homogeneous monolayer adsorption of Cr(VI) on RHC-Mag-2. In addition, a dimensionless separation factor R_L, which was used to reflect the adsorption process, was calculated based on the Langmuir adsorption parameter b [54]:

$$R_L = \frac{1}{1+bC_0}, \tag{7}$$

where b is the Langmuir constant (L·mg^{-1}) and C_0 is the initial adsorbate concentration (mg·L^{-1}). R_L describes the tendency of the adsorption process to be irreversible (R_L=0), favorable (0<R_L<1), linear (R_L=1), or unfavorable (R_L>1).

The R_L values obtained in our experiment were all between 0 and 1, suggesting that RHC-Mag-2 was a favorable adsorbent for Cr(VI). The q_m values were 150.830, 153.374, and 157.729 mg·g^{-1}, which corresponded to 298, 308, and 318 K, respectively. A comparison of the maximum Cr(VI) removal capacity of RHC-Mag-2 with previously reported carbon-based materials (Table 2) revealed that RHC-Mag-2 exhibited a comparable or considerably greater Cr(VI) removal capacity than other previously reported absorbents. This result indicates that RHC-Mag-2 is a promising candidate for the decontamination of chromium-polluted water.

2-5. Thermodynamic Studies

The thermodynamic parameters free energy change (ΔG^0), entropy change (ΔS^0), and enthalpy change (ΔH^0) were calculated using the following equations [57]:

$$\Delta G^0 = -RT \ln K_d \tag{8}$$

$$K_d = \frac{q_e}{C_e} \tag{9}$$

$$\ln K_d = \frac{\Delta S^0}{R} - \frac{\Delta H^0}{RT}, \tag{10}$$

where K_d is the equilibrium constant, R is the gas constant (8.314

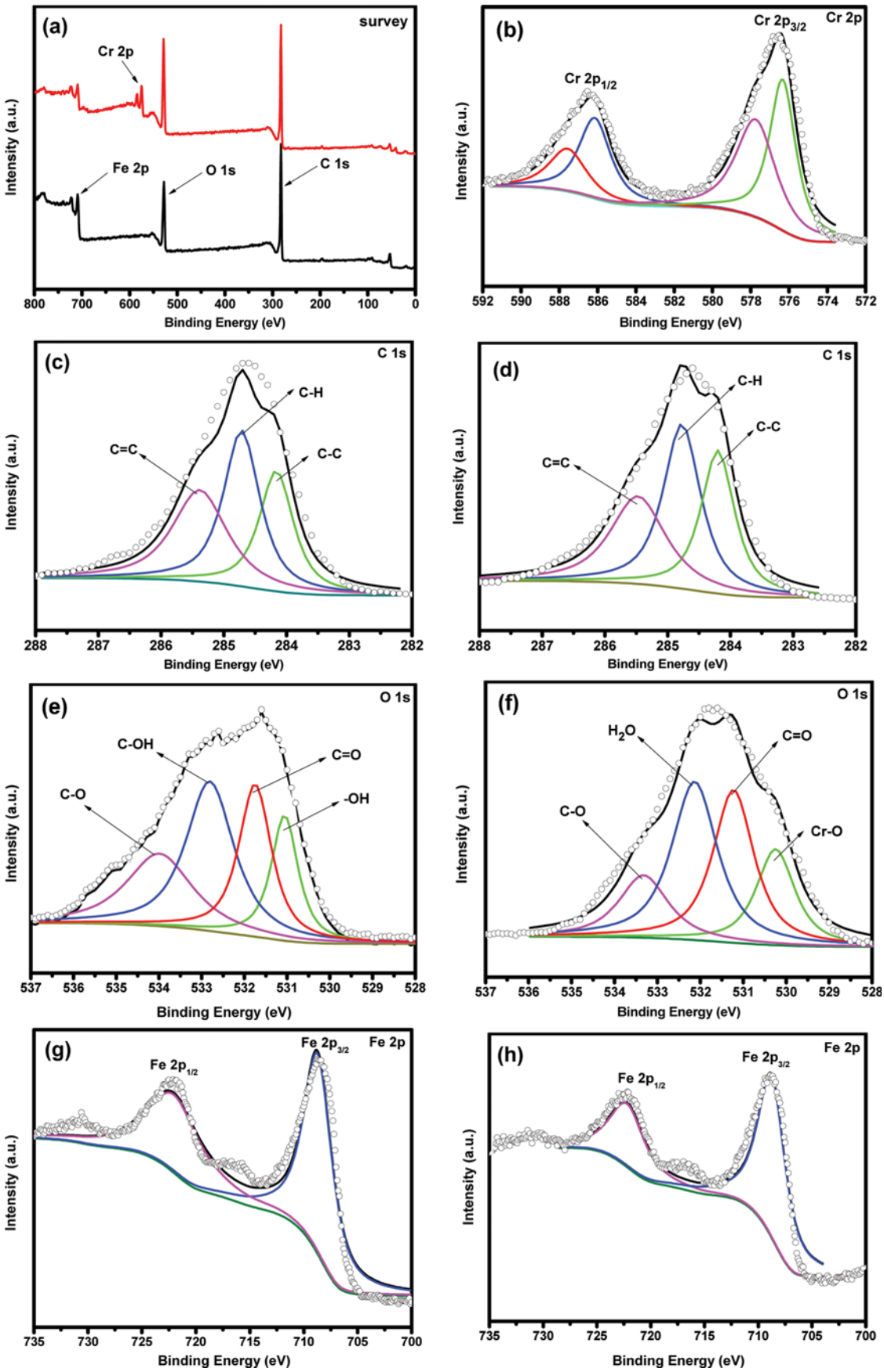

Fig. 8. Survey, Cr 2p, C 1s, O 1s and Fe 2p XPS spectra of RHC-Mag-2 before and after Cr(VI) adsorption.

$J \cdot mol^{-1} \cdot K^{-1}$), and T is the absolute temperature.

The experimental results are shown in Fig. S5 and Table S4. The negative ΔG^0 values showed that the adsorption of Cr(VI) by RHC-Mag-2 was spontaneous. The value of ΔG^0 decreased with increasing temperature. Thus, the adsorption of Cr(VI) onto RHC-Mag-2 was favored by high temperatures. The positive ΔH^0 values of Cr(VI) adsorption on the synthesized adsorbents revealed that the adsorption was endothermic. Furthermore, ΔS^0 with positive values suggests an increasing randomness during Cr(VI) adsorption by RHC-Mag-2 [58,59].

2-6. Adsorption Mechanism

XPS was further employed to investigate the surface chemical states of RHC-Mag-2 before and after Cr(VI) adsorption, and thus elucidate the uptake mechanism of Cr(VI) by RHC-Mag-2. The results of wide-scan XPS characterization are presented in Fig. 8(a). A new peak appeared after adsorption, which was attributed to the photoelectron peak of Cr. This result confirmed the uptake of Cr on the RHC-Mag-2 surface. The Cr2p XPS spectra of RHC-Mag-2 treated with Cr(VI) are shown in Fig. 8(b). The Cr2p peak could be fitted into two components. The peaks at 576.3 and 586.1 eV were related to the Cr $2p_{3/2}$ and Cr $2p_{1/2}$ of Cr(III), respectively, whereas those at 577.7 eV and 587.5 eV were ascribed to the Cr $2p_{3/2}$ and Cr $2p_{1/2}$ of Cr(VI), respectively, demonstrating that Cr(VI) and Cr(III) coexist on the surface of Cr(VI)-adsorbed RHC-Mag-2. This result revealed that some of the adsorbed Cr(VI) was reduced to less toxic Cr(III) during adsorption. As shown in Fig. 8(c), the C 1s peak was deconvoluted to three major components with binding energy peaks at 284.1, 284.7, and 285.3 eV, which corresponded to C-C, C-H, and C=C, respectively. However, minor changes were observed in the XPS spectrum of C 1s (Fig. 8(d)) after interaction with Cr(VI), implying that carbon atoms did not interfere with Cr(VI) adsorption. The peak of the O 1s spectra of RHC-Mag-2 (Fig. 8(e)) was resolved into four major components at 531, 531.7, 532.8, and 534 eV, which corresponded to -OH, C=O, C-OH, and C-O, respectively. The intensity and O 1s components of RHC-Mag-2 significantly changed after Cr(VI) adsorption (Fig. 8(f)). The peak with a binding energy of 530.2 eV could be attributed to the oxygen in the Cr-O bond, which reflected that oxygen atoms participated in Cr(VI) adsorption. To provide further insights into the uptake mechanism of Cr(VI) by RHC-Mag-2, we studied the chemical status of Fe2p species on the adsorbent surface before and after interaction with Cr(VI). As shown in Fig. 8(g), peaks at binding energies of 708.6 eV for Fe $2p_{3/2}$ and 721 eV for Fe $2p_{1/2}$ were observed, which were characteristic of Fe^0 and Fe^{3+}. The peak intensity and area corresponding to Fe^0 and Fe^{3+} slightly decreased after Cr(VI) adsorption (Fig. 8(h)), indicating that Fe^0 was the electron donor involved in the reduction of Cr(VI) to Cr(III).

On the basis of the above analyses, the Cr(VI) removal mechanisms by the as-prepared RHC-Mag-2 are schematically shown in Fig. S6. On the one hand, the hydroxyl groups on the adsorbents were protonated at low pH, and negatively charged Cr(VI) was adsorbed onto the RHC-Mag-2 surface via electrostatic attraction. On the other hand, a redox reaction occurred between Cr(VI) and RHC-Mag-2. The presence of ZVI acting as an electron donor could be responsible for the reduction of Cr(VI) to Cr(III). Some other mechanisms, such as physical adsorption or ion exchange, might also play an important role.

CONCLUSIONS

An RH-derived magnetic carbon adsorbent was successfully prepared by using a simple carbon-thermal method. Given its porous structure, high surface area, and good magnetic properties, the resulting RHC-Mag-2 exhibited a large adsorption capacity and magnetic separation performance. The results revealed that the adsorption behavior of Cr(VI) followed the pseudo-second-order model and Langmuir isotherm. Overall, the waste RH-derived magnetic carbon adsorbent is an attractive candidate for the removal of Cr(VI) from aqueous systems.

ACKNOWLEDGEMENTS

Financial support from the National Natural Science Foundation of China (21446001), the Program for Liaoning Innovative Research Team in University (LT2013012) and the Program for Liaoning Excellent Talents in University (LJQ2014056) is highly appreciated.

SUPPORTING INFORMATION

Additional information as noted in the text. This information is available via the Internet at http://www.springer.com/chemistry/journal/11814.

REFERENCES

1. V. K. Gupta, R. Jain, A. Mittal, T. A. Saleh, A. Nayak, S. Agarwal and S. Sikarwar, *Mater. Sci. Eng. C*, **32**, 12 (2012).
2. T. A. Saleh and V. K. Gupta, *Environ. Sci. Pollut. Res.*, **19**, 1224 (2012).
3. V. K. Gupta, S. K. Srivastava, D. Mohan and S. Sharma, *Waste Manage.*, **17**, 517 (1998).
4. V. K. Gupta, S. Agarwal and T. A. Saleh, *J. Hazard. Mater.*, **185**, 17 (2011).
5. V. K. Gupta, R. Jain, A. Nayak, S. Agarwal and M. Shrivastava, *Mater. Sci. Eng. C*, **31**, 1062 (2011).
6. V. K. Gupta and A. Nayak, *Chem. Eng. J.*, **180**, 81 (2012).
7. T. A. Saleh and V. K. Gupta, *J. Colloid Interface Sci.*, **371**, 101 (2012).
8. H. Khani, M. K. Rofouei, P. Arab, V. K. Gupta and Z. Vafaei, *J. Hazard. Mater.*, **183**, 402 (2010).
9. S. Karthikeyan, V. K. Gupta, R. Boopathy, A. Titus and G. Sekaran, *J. Mol. Liq.*, **173**, 153 (2012).
10. H. B. Gu, S. B. Rapole, Y. D. Huang, D. M. Cao, Z. P. Luo, S. Y. Wei and Z. H. Guo, *J. Mater. Chem. A*, **1**, 2011 (2013).
11. A. A. Hasin, S. J. Gurman, L. M. Murphy, A. Perry, T. J. Smith and P. H. E. Gardiner, *Environ. Sci. Technol.*, **44**, 400 (2010).
12. L. F. Chen, H. W. Liang, Y. Lu, C. H. Cui and S. H. Yu, *Langmuir*, **27**, 8998 (2011).
13. V. K. Gupta, I. Ali, T A. Saleh, A. Nayak and S. Agarwal, *RSC Adv.*, **2**, 6380 (2012).
14. X. J. Hu, J. S. Wang, Y. G. Liu, X. Li, G. M. Zeng, Z. L. Bao, X. X. Zeng, A. W. Chen and F. Long, *J. Hazard. Mater.*, **185**, 306 (2011).

15. A. Mittal, J. Mittal, A. Malviya, D. Kaur and V. K. Gupta, *J. Colloid Interface Sci.*, **342**, 518 (2010).
16. A. Mittal, D. Kaur, A. Malviya, J. Mittal and V. K. Gupta, *J. Colloid Interface Sci.*, **337**, 345 (2009).
17. A. Mittal, J. Mittal, A. Malviya and V. K. Gupta, *J. Colloid Interface Sci.*, **340**, 16 (2009).
18. A. Mittal, J. Mittal, A. Malviya and V. K. Gupta, *J. Colloid Interface Sci.*, **344**, 497 (2010).
19. A. K. Jain, V. K. Gupta, A. Bhatnagar & Suhas, *Sep. Sci. Technol.*, **38**, 463 (2003).
20. V. K. Gupta and I. Ali, *Water Res.*, **35**, 33 (2001).
21. V. K. Gupta, S. Sharma, I. S. Yadav and D. Mohan, *J. Chem. Technol. Biotechnol.*, **71**, 180 (1998).
22. T. A. Saleh, S. Agarwal and V. K. Gupta, *Appl. Catal. B*, **106**, 46 (2011).
23. V. K. Gupta, R. Kumar, A. Nayak, T. A. Saleh and M. A. Barakat, *Adv. Colloid Interface Sci.*, **193-194**, 24 (2013).
24. V. K. Gupta, P. Singh and N. Rahman, *J. Colloid Interface Sci.*, **275**, 398 (2004).
25. V. K. Gupta, B. Gupta, A. Rastogi, S. Agarwal and A. Nayak, *Water Res.*, **45**, 4047 (2011).
26. V. K. Gupta, A. Mittal, D. Jhare and J. Mittal, *RSC Adv.*, **2**, 8381 (2012).
27. V. K. Gupta, I. Ali, V. K. Saini, T. V. Gerven, B. V. Bruggen and C. Vandecasteele, *Ind. Eng. Chem. Res.*, **44**, 3655 (2005).
28. L. L. Wang, Y. P. Guo, Y. C. Zhu, Y. Li, Y. N. Qu, C. G. Rong, X. Y. Ma and Z. C. Wang, *Bioresour. Technol.*, **101**, 9807 (2010).
29. K. S. Low, C. K. Lee and A. Y. Ng, *J. Environ. Sci. Health*, **32**, 1849 (1997).
30. Y. P. Guo, J. R. Qi, S. F. Yang, K. F. Yu, Z. C. Wang and H. D. Xu, *Mater. Chem. Phy.*, **78**, 132 (2002).
31. N. R. Bishnoi, M. Bajaj, N. Sharma and A. Gupta, *Bioresour. Technol.*, **91**, 305 (2004).
32. Y. Li, S. M. Zhu, Q. L. Liu, Z. X. Chen, J. J. Gu, C. L. Zhu, T. Lu, D. Zhang and J. Ma, *Water Res.*, **47**, 4188 (2013).
33. D. H. K. Reddy and S. M. Lee, *Adv. Colloid Interface Sci.*, **201-202**, 68 (2013).
34. X. D. Zhu, Y. C. Liu, C. Zhou, G. Luo, S. C. Zhang and J. M. Chen, *Carbon*, **77**, 627 (2014).
35. L. H. Zhang, Q. Sun, D. H. Liu and A. H. Lu, *J. Mater. Chem. A*, **1**, 9477 (2013).
36. H. B. Gu, D. W. Ding, P. Sameer, J. Guo, N. Yerra, Y. D. Huang, Z. P. Luo, T. C. Ho, N. Haldolaarachchige, D. P. Young, A. Khasanov, Z. H. Guo and S. Y. Wei, *ECS Solid State Letters*, **2**(12), M65 (2013).
37. X. D. Zhu, Y. C. Liu, G. Luo, F. Qian, S. C. Zhang and J. M. Chen, *Environ. Sci. Technol.*, **48**, 5840 (2014).
38. B. Qiu, H. B. Gu, X. R. Yan, J. Guo, Y. R. Wang, D. Z. Sun, Q. Wang, M. Khan, X. Zhang, B. L. Weeks, D. P. Young, Z. H. Guo and S. Y. Wei, *J. Mater. Chem. A*, **2**, 17454 (2014).
39. B. S. Ndazi, S. Karlsson, J. V. Tesha and C. W. Nyahumwa, *Composites*, **38**, 925 (2007).
40. S. Chowdhury, R. Mishra, P. Saha and P. Kushwaha, *Desalination*, **265**, 159 (2011).
41. L. Lin, S. R. Zhai, Z. Y. Xiao, N. Liu, Y. Song, B. Zhai and Q. D. An, *Bioresour. Technol.*, **125**, 172 (2012).
42. L. Lin, S. R. Zhai, Z. Y. Xiao, Y. Song, Q. D. An and X. W. Song, *Bioresour. Technol.*, **136**, 437 (2013).
43. Y. Chen, S. R. Zhai, N. Liu, Y. Song, Q. D. An and X. W. Song, *Bioresour. Technol.*, **144**, 401 (2013).
44. J. J. Ma, L. C. Zhou, W. F. Dan, H. Zhang, Y. M. Shao, C. Bao and L. Y. Jing, *J. Colloid Interface Sci.*, **446**, 298 (2015).
45. H. Y. Zhu, Y. Q. Fu, R. Jiang, J. H. Jiang, L. Xiao, G. M. Zeng, S. L. Zhao and Y. Wang, *Chem. Eng. J.*, **173**, 494 (2011).
46. W. F. Liu, J. Zhang, C. L. Zhang and L. Ren, *Chem. Eng. J.*, **189-190**, 295 (2012).
47. L. Z. Zhuang, Q. H. Li, J. S. Chen, B. B. Ma and S. X. Chen, *Chem. Eng. J.*, **253**, 24 (2014).
48. H. Guo, S. F. Zhang, Z. N. Kou, S. R. Zhai, W. Ma and Y. Yang, *Carbohydr. Polym.*, **115**, 177 (2015).
49. B. Qiu, Y. R. Wang, D. Z. Sun, Q. Wang, X. Zhang, B. L. Weeks, R. O'Connor, X. H. Huang, S. Y. Wei and Z. H. Guo, *J. Mater. Chem. A*, **3**, 9817 (2015).
50. T. S. Anirudhan and P. Senan, *Sep. Sci. Technol.*, **46**, 1430 (2011).
51. Z. G. Liu and F. S. Zhang, *Bioresour. Technol.*, **101**, 2562 (2010).
52. I. Langmuir, *J. Am. Chem. Soc.*, **40**, 1361 (1918).
53. J. H. Wang, X. L. Yin, W. Tang and H. R. Ma, *Korean J. Chem. Eng.*, **32**, 1889 (2015).
54. K. R. Hall, L. C. Eagleton, A. Acrivos and T. Vermeulen, *Ind. Eng. Chem. Fundam.*, **5**, 212 (1966).
55. C. L. Wu, J. Fan, J. H. Jiang and J. J. Wang, *RSC Adv.*, **5**, 47165 (2015).
56. S. Nethaji, A. Sivasamy and A. B. Mandal, *Bioresour. Technol.*, **134**, 94 (2013).
57. A. Sari and M. Tuzen, *J. Hazard. Mater.*, **160**, 349 (2008).
58. M. M. Zhang, Y. G. Liu, T. T. Li, W. H. Xu, B. H. Zheng, X. F. Tan, H. Wang, Y. M. Guo, F. Y. Guo and S. F. Wang, *RSC Adv.*, **5**, 46955 (2015).
59. L. F. Zhang, W. Xia, X. Liu and W. Q. Zhang, *J. Mater. Chem. A*, **3**, 331 (2015).

Supporting Information

Removal of Cr(VI) from aqueous solution by rice husk derived magnetic sorbents

Yuan Fan, Ruifeng Yang†, Zhimin Lei, Na Liu, Jialiang Lv, Shangru Zhai†, Bin Zhai, and Lei Wang

Faculty of Light Industry and Chemical Engineering, Dalian Polytechnic University, Dalian 116034, China
(*Received 26 August 2015 • accepted 17 November 2015*)

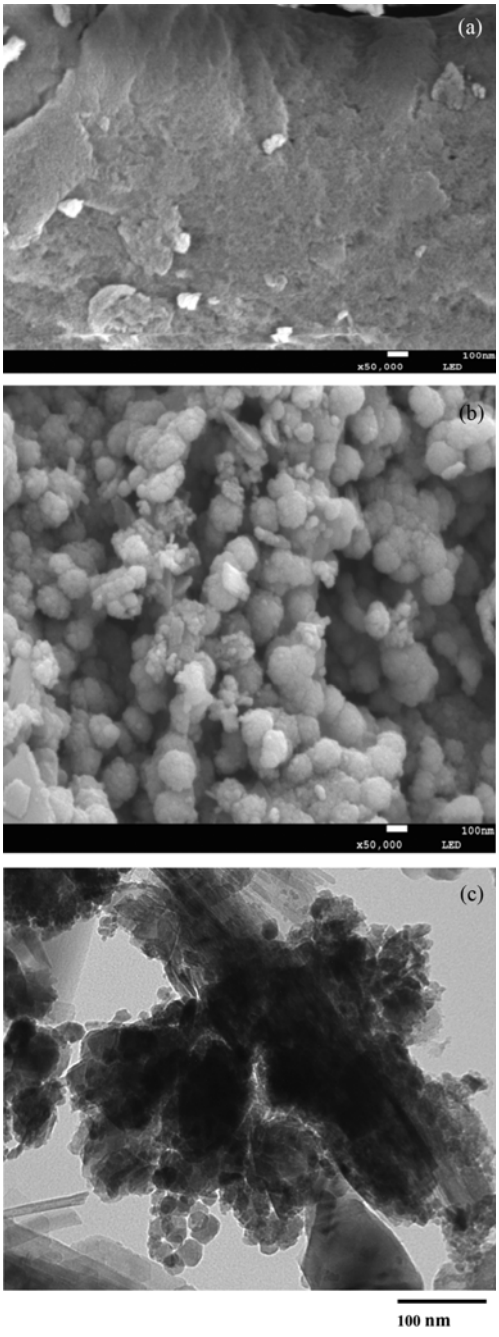

Fig. S1. SEM images of (a) RH, (b) RHC-Mag-2 and (c) TEM image of RHC-Mag-2.

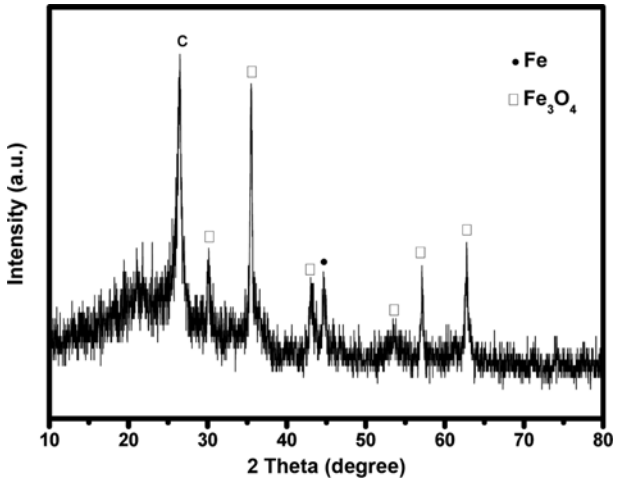

Fig. S2. XRD pattern of RHC-Mag-2.

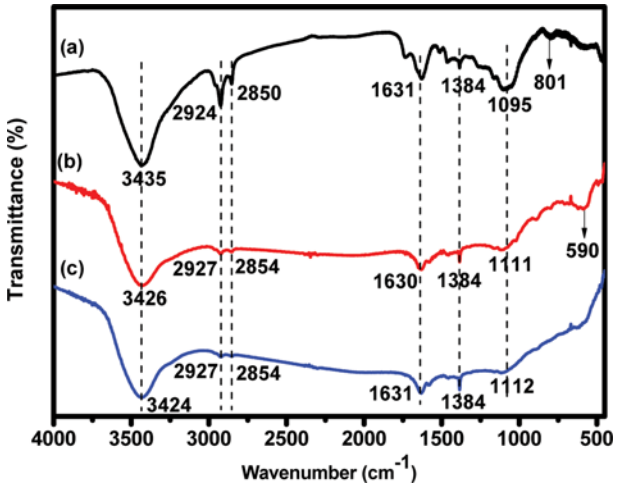

Fig. S3. FT-IR spectra of (a) RH, (b) RHC-Mag-2 and (c) RHC-Mag-2 after adsorption.

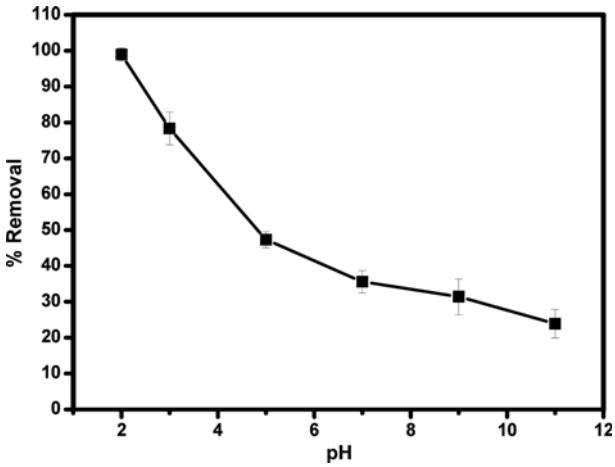

Fig. S4. Effect of the pH on the adsorption of Cr(VI) onto RHC-Mag-2 (adsorbent dose, 0.02 g; volume, 20 mL; initial Cr(VI) concentration, 50 mg/L; contact time, 3 h and temperature, 298 K).

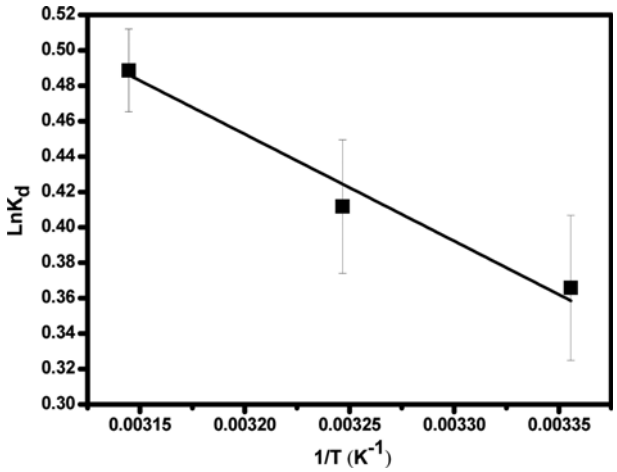

Fig. S5. Relationship curve between ln K_d and 1/T.

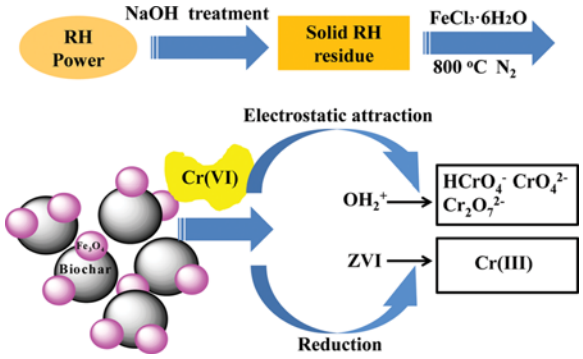

Fig. S6. Magnetic porous sorbents that can highly efficient remove toxic Cr(VI) ions were prepared by a simple carbonthermal processing of NaOH treated rice husk.

Table S1. The textural parameters of the RH and RH-Mag-2

Sample	Specific surface area ($m^2\ g^{-1}$)	Pore volume ($cm^3\ g^{-1}$)	Average pore diameter (nm)
RH	9.1	0.01	8.36
RH-Mag-2	134.1	0.26	4.99

Table S2. Adsorption isotherm constants and correlation coefficients for adsorption of Cr(VI) at different Fe^{3+} ratio

Isotherms	Parameters	Samples		
		RHC-Mag-0.5	RHC-Mag-1	RHC-Mag-2
Langmuir	Q_m (mg g^{-1})	96.993	126.582	150.830
	b (L mg^{-1})	0.6384	0.6124	0.6344
	R^2	0.9993	0.9982	0.9997
Freundlich	K_f (L g^{-1})	46.338	49.814	60.126
	1/n	0.1529	0.2331	0.2172
	R^2	0.9818	0.8147	0.8587

Table S3. Isotherm parameters for adsorption of Cr(VI) onto RH-Mag-2 at different temperatures

Isotherms	Parameters	Temperature (K)		
		298	308	318
Langmuir	Q_m (mg g^{-1})	150.830	153.374	157.729
	b (L mg^{-1})	0.6344	0.5262	0.5040
	R_L	0.005-0.030	0.006-0.036	0.006-0.038
	R^2	0.9997	0.9997	0.9999
Freundlich	K_f (L g^{-1})	60.126	69.349	80.490
	1/n	0.2172	0.1817	0.1519
	R^2	0.8587	0.7667	0.7965

Table S4. Thermodynamic parameters for the adsorption of Cr(VI) onto RH-Mag-2

ΔH^0 (KJ mol^{-1})	ΔS^0 (J mol^{-1} K^{-1})	ΔG^0 (kJ mol^{-1})		
		298 K	308 K	318 K
5.023	19.837	−0.906	−1.054	−1.292